Efficiency Optimization of a 100-W 500 000-r/min Permanent-Magnet Machine Including Air-Friction Losses

Jorma Luomi, *Member, IEEE*, Christof Zwyssig, *Student Member, IEEE*, Andreas Looser, *Student Member, IEEE*, and Johann W. Kolar, *Senior Member, IEEE*

***Abstract*—This paper proposes a method for the efficiency optimization of ultrahigh-speed permanent-magnet machines. Analytical methods are applied for the modeling of the machine that is equipped with a diametrically magnetized rotor and a slotless stator. The outer dimensions of the machine are design constraints, and the internal dimensioning is optimized for minimum losses. The air-friction losses are taken into account in addition to the usual iron, copper, and eddy-current losses. Laminated silicon–iron or laminated amorphous iron is used as the stator core material. The results show that air-friction losses influence the optimum design considerably, leading to a small rotor diameter at high speeds. The loss minimization and the amorphous iron core make it possible to reduce the calculated losses by 63% as compared to a machine design not considering air-friction losses. The resulting efficiency is 95% for a 100-W 500 000-r/min machine excluding bearing losses. Experimental results are shown to illustrate the validity of the method.**

***Index Terms*—Air friction, high speed, optimization, permanent magnet (PM).**

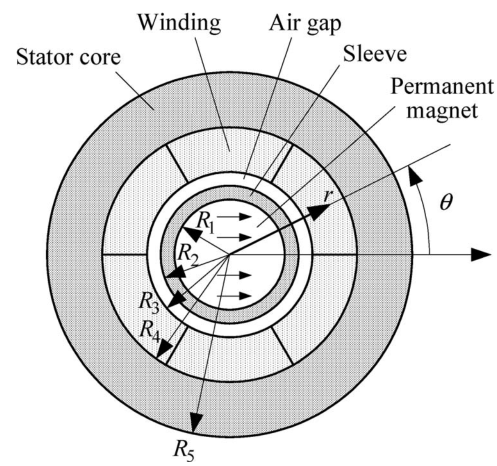

Fig. 1. Machine cross section and symbol definitions: diametrically magnetized cylindrical PM rotor inside a slotless stator.

I. Introduction

ULTRAHIGH-SPEED electrical-drive systems are developed for new emerging applications, such as generators/starters for micro gas turbines, turbo-compressor systems, drills for medical applications, and spindles for machining. Typically, the power ratings of these applications range from a few watts to a few kilowatts and the speeds from a few tens of thousands revolutions per minute up to a million revolutions per minute [1]. Recently, a 100-W 500 000-r/min permanent-magnet (PM) machine has been designed and investigated experimentally [2], [3]. For such high speeds, the mechanical-rotor construction and the minimization of high-frequency losses are the main challenges. This machine has a diametrically magnetized cylindrical Sm_2Co_{17} PM encased in a titanium sleeve for sufficiently low mechanical stresses on the magnet. The slotless stator core consists of 168-μm silicon–iron laminations, and the three-phase air-gap winding is made of litz wire with 0.071-mm strands for low copper losses. The cross section of the machine is shown in Fig. 1.

In designing an ultrahigh-speed machine, it is important to optimize the efficiency—i.e., minimize the losses—when the outer dimensions of the machine are design constraints. Previously, such optimizations have been based on resistive losses in the stator winding and iron losses in the stator core [4] and, in addition, eddy-current losses in the rotor [5]. However, air-friction losses are an important part of the total losses in an ultrahigh-speed machine [2]. Therefore, these losses should also be taken into account in the optimization.

This paper proposes a method for the loss minimization of ultrahigh-speed PM machines including air-friction losses. Analytical methods are applied for the modeling. In the following, models are first presented for the magnetic field and the loss components. Then, the optimization procedure is briefly described, and results of the loss minimization are shown. Finally, experimental results are presented.

II. Magnetic Field and Torque

A solution of the magnetic field is required for analyzing the operating point, resistive losses, eddy-current losses, and iron losses. Today, numerical analysis based on the finite-element

Paper 2008-EMC-049.R1, presented at the 2007 Industry Applications Society Annual Meeting, New Orleans, LA, September 23–27, and approved for publication in the IEEE Transactions on Industry Applications by the Electric Machines Committee of the IEEE Industry Applications Society. Manuscript submitted for review July 23, 2008 and released for publication February 7, 2009. First published May 19, 2009; current version published July 17, 2009.

J. Luomi is with the Department of Electrical Engineering, Helsinki University of Technology, 02150 Espoo, Finland (e-mail: jorma.luomi@tkk.fi).

C. Zwyssig is with Celeroton, 8092 Zürich, Switzerland (e-mail: christof.zwyssig@celeroton.com).

A. Looser and J. W. Kolar are with the Power Electronic Systems Laboratory, Eidgenoessische Technische Hochschule Zürich, 8092 Zürich, Switzerland (e-mail: kolar@lem.ee.ethz.ch).

Digital Object Identifier 10.1109/TIA.2009.2023492

(FE) method is the standard methodology for such calculations. However, analytical models can give more insight into the problem; they are computationally efficient in many cases and result in smooth solutions, which is favorable in optimization. Analytical solutions of the magnetic field have been derived for PM machines with radially magnetized magnets in the rotor, e.g., [6], [7]. Solutions for machines with diametrically magnetized rotors have been presented in [8] and [9]. Usually, the permeability of the stator iron core has been assumed infinite when the magnetic field of a PM machine is solved analytically, and the solution is restricted to the air gap and the rotor. However, an analytical model of the magnetic field in the stator core can be used for the evaluation of the iron-loss distribution [10].

The cross section of the two-pole machine is shown in Fig. 1. The symbols for the radial dimensions are as follows: radius of the PM R_1, outer radius of the rotor sleeve R_2, inner radius of the stator winding R_3, and inner and outer radii of the stator core R_4 and R_5, respectively. The length of the stator core is denoted by L, and the mechanical air gap is $\delta = R_3 - R_2$. The diametrically magnetized PM has a uniformly distributed remanence flux density B_{rem} and a relative recoil permeability μ_{r1}. The region between the PM and the stator core $(R_1 < r < R_4)$ is nonferromagnetic and forms an equivalent air gap for the magnetic field. The relative permeability of the stator core is μ_{r5}. The machine is to be fed by an inverter using field-oriented control. The stator-current component in the direction of the PM flux is controlled to zero, giving maximum-torque-per-ampere control due to the nonsalient rotor design.

Analytical solution of the magnetic field is particularly simple for the machine type considered. In the Appendix, a solution is presented for the entire cross section of the machine, and the evaluation of the torque based on the field solution is also described. The analytical model is based on solving only the magnetic field produced by the PM in a coordinate system fixed to the rotor. The magnetic field contribution caused by the stator current can be added to the model in a fashion similar to [11]. Furthermore, the variation of this field contribution induces eddy currents in the conducting rotor sleeve, which can also be included in the model [12], [13]. However, the magnetic field of a PM machine with an air-gap winding is mainly produced by the PM, and the influence of the stator winding is very small [3]. Hence, the efficiency optimization can be carried out without modeling the magnetic field contribution caused by the stator current.

It is typical of ultrahigh-speed PM machines with a slotless design that the magnetic flux density does not reach values causing magnetic saturation in the iron core. If magnetic saturation occurs, it is easy to replace the analytical model with FE analysis in the optimization.

III. Loss Models

A. Copper Losses

The frequency of the stator current is high (8.3 kHz in the 500 000-r/min machine). Therefore, eddy currents increase the copper losses of the stator winding. In addition to the stator current, the air-gap flux causes considerable eddy-current losses in the winding due to the slotless design of the stator. In order to reduce the losses, the winding is made of litz wire.

The copper losses consist of the current-dependent resistive losses $P_{\mathrm{Cu},s}$ in the stator winding, which include the influence of the skin effect and of the proximity-effect losses $P_{\mathrm{Cu},p}$, which are mainly due to the eddy currents induced by the magnetic field of the PM. The copper losses are

$$P_{\mathrm{Cu}} = P_{\mathrm{Cu},s} + P_{\mathrm{Cu},p} = I^2 F + G\frac{\hat{H}^2}{\sigma} \tag{1}$$

where I is the rms stator current, $\hat{H}$ is the peak magnetic field strength in the winding, σ is the conductivity of the conductor, and the coefficients F and G include the effects of the eddy currents. The Ferreira method was chosen for the modeling of the eddy-current effects; the coefficients F and G are calculated based on the frequency, the conductivity, and the geometry of the winding arrangement, as described in [14]. At significantly higher frequencies or larger strand diameters, the accuracy could be increased by using a method based on function fitting for the calculation of the proximity-effect losses [15].

B. Iron Losses

The iron losses are calculated as an integral over the iron volume V_{Fe} using the Steinmetz equation

$$P_{\mathrm{Fe}} = \int_{V_{\mathrm{Fe}}} C_m \cdot f^{\alpha} \cdot \hat{B}^{\beta} dV \tag{2}$$

where f is the frequency and $\hat{B}$ is the peak magnetic flux density. The coefficients C_m, α, and β are taken from the manufacturer's data sheets for the frequency range to be considered.

C. Air-Friction Losses

For simple geometries, such as cylinders and disks, air-friction losses can be calculated analytically with friction coefficients based on empirical data [16]. In the following, only the air gap is taken into account in the calculation of the air-friction losses, and the losses at the end caps are omitted.

The air-friction losses of a long rotating cylinder encased in a stationary hollow cylinder are

$$P_{f,\mathrm{air}} = c_f \pi \rho_{\mathrm{air}} \omega^3 R_2^4 L \tag{3}$$

where ρ_{air} is the density of the air, ω is the angular speed, R_2 is the radius of the cylinder, and L is the length of the cylinder. The friction coefficient c_f depends on the radius of the cylinder, the air gap δ, and the Reynolds and the Taylor numbers, which are defined as

$$Re = \frac{R_2^2 \omega}{\nu} \quad Ta = \frac{R_2 \omega \delta}{\nu}\sqrt{\frac{\delta}{R_2}} \tag{4}$$

where ν is the kinematic viscosity of air. The flow stability depends on the Taylor number; the flow can be divided into laminar Couette flow $(Ta < 41.3)$, laminar flow with Taylor vortices $(41.3 < Ta < 400)$, and turbulent flow $(Ta > 400)$.

For laminar Couette flow, the friction coefficient can be determined analytically, but measurements show discrepancies with the theoretical values. Therefore, empirical data are usually used, and correction factors are applied to adapt for different geometries [16]. For the air gap of the machine under investigation, the friction coefficient

$$c_f = \frac{1.8}{Re}\left(\frac{\delta}{R_2}\right)^{-0.25}\frac{R_3^2}{R_3^2 - R_2^2} \tag{5}$$

can be used. Beyond the transition point from laminar flow to flow with Taylor vortices, measurements show a friction coefficient

$$c_f \propto Ta^{-0.2}. \tag{6}$$

This model for air-friction losses has been experimentally validated in [16].

D. Other Losses and Shaft Torque

The nonsinusoidal distribution of the stator winding causes spatial harmonics in the magnetic field, and time-harmonics are present in the stator voltage due to the inverter supply, but the eddy-current losses in the rotor of a slotless PM machine are generally very low, as shown in [5]. Therefore, the rotor losses are ignored in the following. Furthermore, it is to be noted that the bearing losses are not considered in the efficiency optimization of the machine, since they are usually more dependent on the application than on the inner dimensions of the motor.

The machine is to be optimized for a given mechanical shaft torque T_m. When the proximity-effect, iron, and air-friction losses are taken into account, the electromagnetic torque can be calculated by

$$T_e = T_m + \frac{P_{\mathrm{Cu},p} + P_{\mathrm{Fe}} + P_{f,\mathrm{air}}}{\omega}. \tag{7}$$

IV. Mechanical Model

A 2-D mechanical model is used for the rotor. The stresses of the rotor construction with the PM shrink fitted into a titanium sleeve have been analyzed in [3]. The following specifications have to be fulfilled in the entire operation region.

1) The torque transfer and low eccentricity are guaranteed by allowing no lift off of the sleeve. Thus, the radial stress at the interface between the PM and the sleeve has to be negative, which is most critical at the maximum speed.
2) Stresses in the entire PM have a safety margin of 30% to the tensile strength of Sm_2Co_{17} (120 MPa). The most critical stress occurs at the maximum speed in the center of the magnet.
3) Stresses in the entire sleeve have a safety margin of 50% to the tensile strength of titanium (900 MPa). The most critical stress occurs at the maximum speed on the inner side of the sleeve.
4) The sleeve has a minimum thickness (0.25 mm) for manufacturability reasons.

V. Optimization

A. Loss Minimization

The goal is to minimize the total losses obtained from (1)–(3), i.e., the objective function is

$$P_d = P_{\mathrm{Cu}} + P_{\mathrm{Fe}} + P_{f,\mathrm{air}}. \tag{8}$$

The losses are minimized for a given rotational speed n and shaft torque T_m. The outer radius R_5 and length L of the stator core are kept constant (or changed in an outer iteration). The independent variables are the magnet radius R_1, the air gap δ, and the inner radius of the stator core R_4.

The loss minimization is constrained in order to obtain a geometrically, mechanically, and magnetically feasible design. The sleeve thickness $R_2 - R_1$ is kept at the minimum value given by the mechanical analysis. The minimum value for the air gap δ is 0.2 mm, and the minimum value for the thickness of the stator core $(R_5 - R_4)$ is 1 mm. In addition, the flux density in the iron core is limited to a maximum value (1.3 T for a silicon–iron stack and 1.1 T for an amorphous iron stack). In the results presented in this paper, a constant temperature of 120 °C is assumed for the stator winding.

Many different methods can be used for solving the minimization problem. A straightforward choice is the Nelder–Mead simplex method included in the MATLAB software as the function fminsearch. The constraints can be included in this derivative-free minimization method by giving the objective function a high value if the design is not feasible.

B. Litz-Wire Optimization

The strand diameter of the litz wire influences only the copper losses. During the loss minimization, the strand diameter giving the lowest copper losses is selected for every feasible design. Making the strands thinner decreases the eddy currents but increases the resistive losses if the winding fill factor decreases.

The winding fill factor is given by

$$k_{\mathrm{Cu}} = k_{\mathrm{Cu},t}k_{\mathrm{Cu},s}. \tag{9}$$

Here, the turn fill factor $k_{\mathrm{Cu},t}$ is defined as the ratio of the area occupied by the litz wires to the total cross-sectional area of the winding, and the strand packing factor $k_{\mathrm{Cu},s}$ is the ratio of the copper area of the strands in the wire to the area of the wire. The turn fill factor is assumed to be constant, whereas the strand packing factor is a function of the strand diameter. Fig. 2 shows the strand packing factors $k_{\mathrm{Cu},s}$ for various strand diameters obtained from the manufacturer's data [17].

VI. Results

A. Mechanical-Rotor Model

The thickness of the rotor sleeve and the interference fit required were calculated using the mechanical model. The results are shown in Fig. 3 for a rotor with a maximum speed of 500 000 r/min. For small rotor radii, the sleeve thickness is

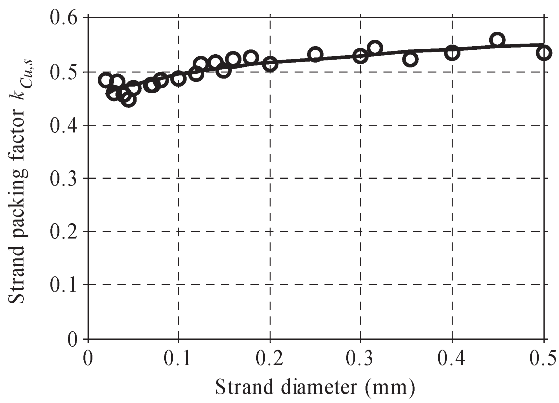

Fig. 2. Strand packing factor $k_{\mathrm{Cu},s}$ as function of strand diameter. (Markers) Manufacturer's data. (Line) Fitted curve.

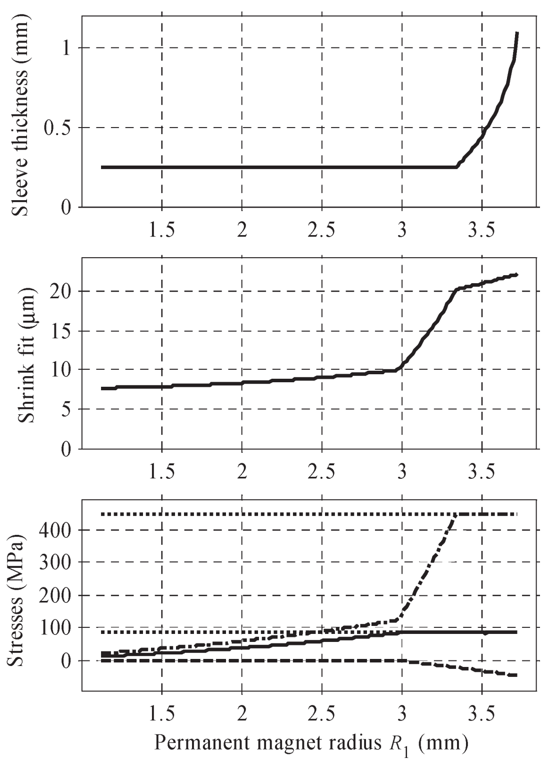

Fig. 3. Results of mechanical analysis as function of rotor radius at 500 000 r/min. The first subfigure shows the sleeve thickness $R_2 - R_1$, the second subfigure shows the shrink fit, and the third subfigure shows (solid) radial stress in the center of the PM, (dashed) radial stress at the interface (R_1), (dash-dotted) tangential stress in the sleeve at R_1, and (dotted) stress limits in the magnet and sleeve.

at the minimum value defined by the manufacturability; the shrink fit ensures that the sleeve does not lift off. At 3-mm magnet radius, the stress in the magnet reaches its limit, and the shrink fit has to be enforced to guarantee the safety margin to the tensile strength of Sm_2Co_{17}. At 3.3 mm, the stress in the titanium sleeve reaches its limit, and the sleeve thickness has to be increased in order to guarantee the safety margin to the tensile strength of titanium.

B. Fixed Outer Dimensions

The parameters used in the efficiency optimization are given in Table I. Figs. 4 and 5 show the dependence of the losses

TABLE I
PARAMETERS USED IN EFFICIENCY OPTIMIZATION

Symbol	Quantity	Value
Permanent magnet		
B_{rem}	Remanence flux density	1.1 T
μ_{r1}	Relative recoil permeability	1.05
Silicon-iron laminations (168 µm)		
μ_{r5}	Relative permeability	1860
C_m	Steinmetz coefficient	21.8 W/m^3
α	Steinmetz coefficient	1.42
β	Steinmetz coefficient	1.50
Amorphous iron (Metglas magnetic alloy 2605SA1)		
μ_{r5}	Relative permeability	35100
C_m	Steinmetz coefficient	0.94 W/m^3
α	Steinmetz coefficient	1.53
β	Steinmetz coefficient	1.72
Air		
ρ_{air}	Density	1.29 kg/m^3
ν	Kinematic viscosity	0.000014 m^2/s

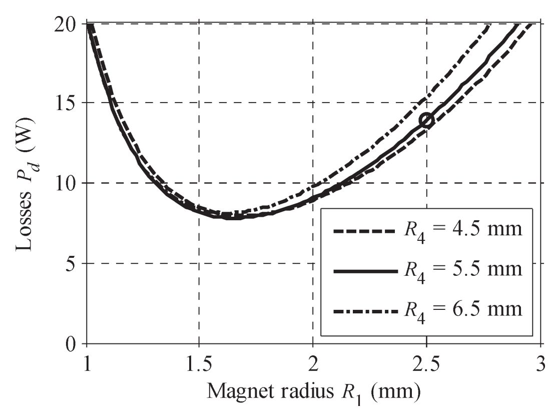

Fig. 4. Losses of the machine with fixed outer dimensions of the stator core ($R_5 = 8$ mm, $L = 15$ mm) and a shaft power of 100 W at a rotational speed of 500 000 r/min for variable magnet radius R_1 and various values of the inner radius R_4 of the stator core. The circle shows the value for the existing machine with $R_4 = 5.5$ mm and $R_1 = 2.5$ mm [3].

on the internal radial dimensions of the machine. The outer dimensions of an existing machine were used ($R_5 = 8$ mm and $L = 15$ mm [3]), and the stator core material was laminated silicon–iron. The sleeve thickness was fixed to the original value (0.5 mm) and so were the air gap (0.5 mm) and the strand diameter of the litz wire (0.071 mm). In Fig. 4, the total losses are shown as a function of the magnet radius R_1 for various values of the inner radius R_4 of the stator core. The individual loss components are shown in Fig. 5 for the original value $R_4 = 5.5$ mm. It is shown that the total losses depend strongly on the radius of the PM, whereas the sensitivity to the inner diameter of the core is low if the radius of the PM is appropriately chosen.

The minimum of the losses is about 9 W, and it is obtained at $R_4 = 5.3$ mm and $R_1 = 1.7$ mm. The original machine design is based on the values $R_4 = 5.5$ mm and $R_1 = 2.5$ mm [3], and

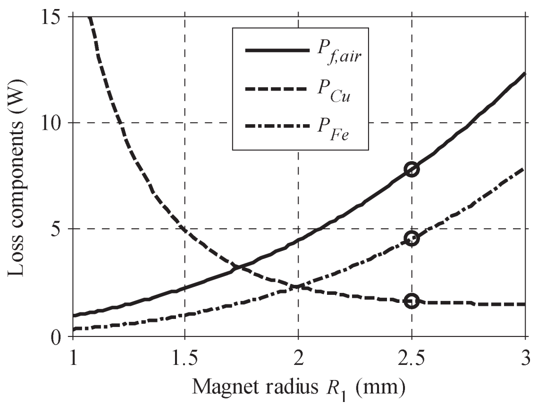

Fig. 5. Loss components of the machine with fixed outer dimensions of the stator core ($R_5 = 8$ mm, $L = 15$ mm) and a shaft power of 100 W at a rotational speed of 500 000 r/min for variable magnet radius R_1 and constant inner radius of the stator core, $R_4 = 5.5$ mm. The circle shows the values for the existing machine with $R_1 = 2.5$ mm [3].

it has 14.2 W of losses. Thus, a reduction of losses by 5.2 W can be obtained by changing the internal radial dimensions of the machine. In this case, the loss reduction is mainly due to the optimization of the magnet radius R_1. The loss reduction achieved by changing the inner radius R_4 of the stator core is about 0.01 W and, thus, negligible.

The optimization leads to a rather expected result: Decreasing the rotor diameter leads to a reduction of the air-friction losses. The iron losses are also reduced, since a smaller magnet radius leads to a lower air-gap flux density in the machine considered. In order to keep the torque constant, the total current of the stator winding has to be increased, leading to increasing copper losses when the magnet radius is decreased. However, a larger amount of air-friction and iron losses can be avoided by decreasing the magnet radius.

The losses of the existing machine obtained with the loss models presented in this paper are shown by circular markers in Figs. 4 and 5. There are small differences between the values shown in this paper and the ones obtained in [2] by means of measurements and separation of losses; these differences originate from the less accurate model used earlier for iron losses and from a small difference in the winding geometry and temperature.

C. Variable Outer Dimensions and Strand Diameter

For improved loss minimization, the sleeve thickness was reduced to the minimum value given by the mechanical analysis ($R_2 - R_1 = 0.25$ mm), and the optimization was based on the three independent variables (R_1, δ, and R_4). In addition, the strand diameter giving lowest copper losses was determined for the litz wire. In all of the following examples, the loss minimization resulted in an air gap value of $\delta = 0.2$ mm, i.e., the minimum value. The optimum strand diameter of the litz wire varied between 0.03 and 0.05 mm, but the influence of small changes in the strand diameter is insignificant, since the proximity-effect losses are much lower than the other loss components.

Fig. 6 shows the magnet radius R_1 and inner radius R_4 of the stator core for the laminated silicon–iron core material. The results are shown for variable outer radius R_5 of the stator core and various values of the core length L. The corresponding total losses are shown in Fig. 7. For the original outer dimensions ($R_5 = 8$ mm and $L = 15$ mm), the losses can be reduced to about 7 W by choosing $R_4 = 5.1$ mm and $R_1 = 1.8$ mm. Thus, the reduction of the air-gap and sleeve thickness allows a loss reduction by 2 W from the result shown in Fig. 4. The contributions of the air-gap and sleeve thickness to this loss reduction are 0.7 and 1.3 W, respectively. The losses can be further reduced by increasing the outer dimensions of the machine.

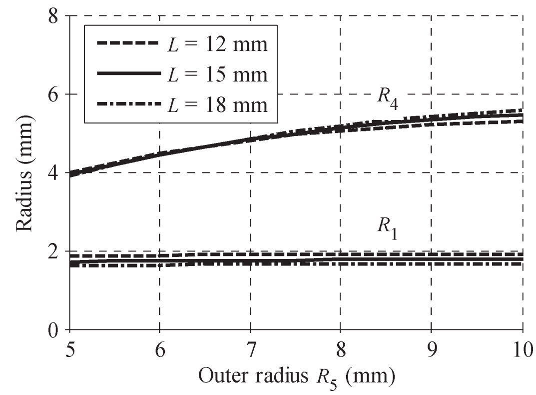

Fig. 6. Optimization results for the silicon–iron core. Magnet radius R_1 and inner radius R_4 of the stator core for variable outer radius R_5 of the stator core and various values of the core length L. The shaft power is 100 W and the rotational speed 500 000 r/min.

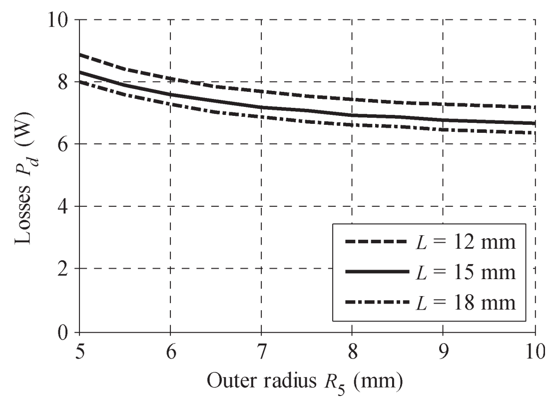

Fig. 7. Optimization results for the silicon–iron core. Total losses P_d for variable outer radius R_5 of the stator core and various values of the core length L. The shaft power is 100 W and the rotational speed 500 000 r/min.

D. Influence of Stator Core Material

Figs. 8 and 9 show the loss-minimization results when the stator core material was laminated amorphous iron (Metglas magnetic alloy 2605SA1). In this case, the iron losses are lower than 10% of the total losses. If the original outer dimensions of the machine are used, a loss reduction to about 5.2 W is possible by choosing $R_4 = 4.5$ mm and $R_1 = 1.9$ mm. The losses of the existing machine (14.2 W) can thus be reduced by 63% without changing the outer dimensions.

It is obvious that, for constant L, the results shown in Figs. 8 and 9 do not depend much on the outer radius R_5 if $R_5 \approx 6$ mm

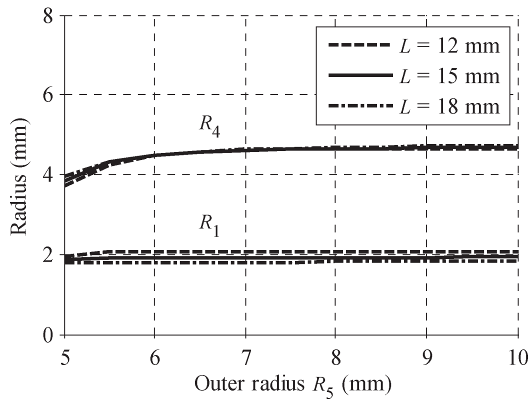

Fig. 8. Optimization results for the amorphous iron core. Magnet radius R_1 and inner radius R_4 of the stator core for variable outer radius R_5 of the stator core and various values of the core length L. The shaft power is 100 W and the rotational speed 500 000 r/min.

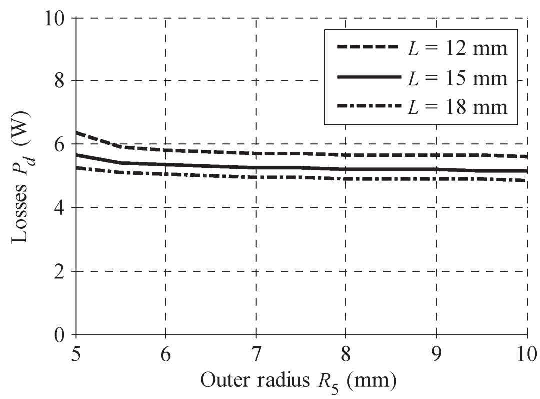

Fig. 9. Optimization results for the amorphous iron core. Total losses P_d for variable outer radius R_5 of the stator core and various values of the core length L. The shaft power is 100 W and the rotational speed 500 000 r/min.

or larger. Thus, the outer diameter of the stator can be reduced from the original value with almost no influence on the losses. The losses are higher at the lowest values of R_5. The loss increase is caused by two constraints used in the optimization: the minimum thickness of the stator core (1 mm) and the maximum flux density allowed in the stator core (1.1 T).

E. Influence of Air-Friction Losses

The air-friction losses (3) are approximately proportional to R_2^4. At high speeds, the inclusion of this loss component in the loss minimization leads to a smaller rotor radius than the one obtained without this loss component. This fact is shown in Figs. 10 and 11 showing the loss-minimization results when the air-friction losses are omitted.

F. Influence of Speed

In order to investigate the influence of the rotational speed on the results, the losses of 100-W motors were minimized in the speed range between 100 000 and 1 000 000 r/min. The core length was fixed to $L = 15$ mm, and the outer radius R_5 of the core was adjusted in such a way that the flux density was 1.1 T (if possible without contradicting the minimum-core-thickness constraint). The results are shown in Figs. 12 and 13. It is obvious that the inclusion of the air-friction losses in the loss minimization leads to very small rotor diameters at the highest speeds. For the power rating considered, the analysis of rotor dynamics would have to be included in the optimization for speeds higher than 500 000 r/min, which finally restricts the reduction of the rotor radius with increasing speed.

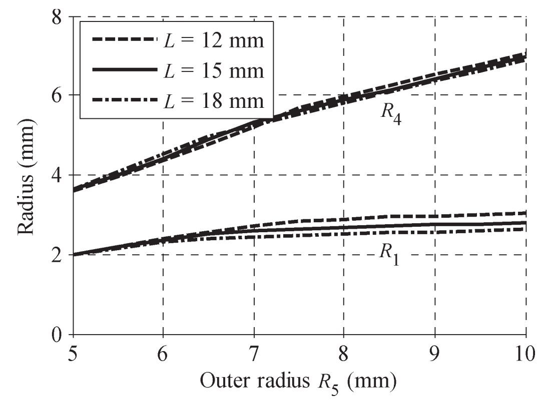

Fig. 10. Optimization results when air-friction losses are omitted. Explanations of curves are as in Fig. 8.

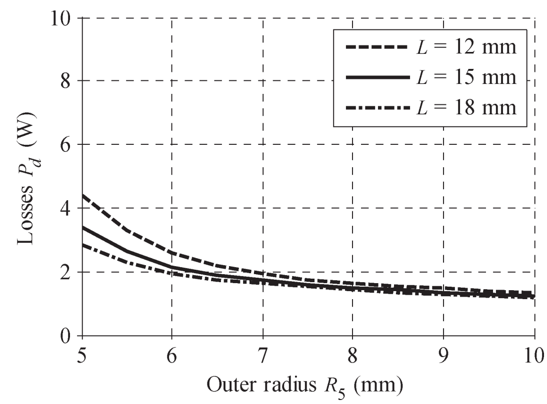

Fig. 11. Optimization results when air-friction losses are omitted. Explanations of curves are as in Fig. 9.

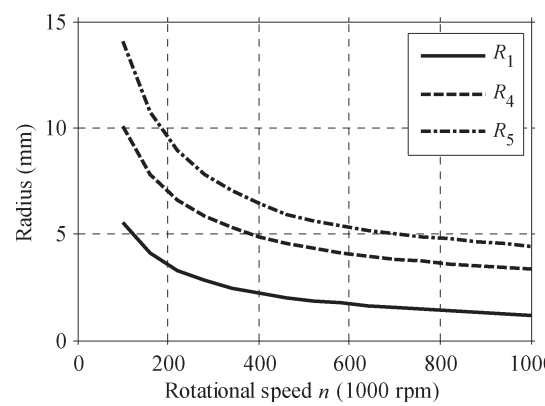

Fig. 12. Magnet radius R_1, and inner radius R_4 and outer radius R_5 of the stator core as functions of the rotational speed n used in the optimization. The shaft power is 100 W and the core length $L = 15$ mm.

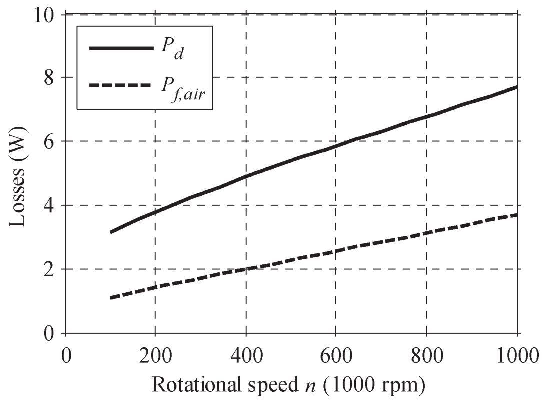

Fig. 13. Total losses P_d and air-friction losses $P_{f,\mathrm{air}}$ as functions of the rotational speed n used in the optimization. The shaft power is 100 W and the core length $L = 15$ mm.

Fig. 14. Stator and rotor of Machine A (100 W, 500 000 r/min), designed without the efficiency optimization including air-friction losses. The active length is 15 mm and the PM diameter is 5 mm.

Fig. 15. Machine B (100 W, 1 000 000 r/min) and its rotor, designed using the efficiency optimization including air-friction losses. The active length is 11.5 mm and the PM diameter is 3 mm.

VII. Experimental Results

A. Hardware

In order to validate the models and the optimization method, experiments were carried out using two machines that were built during this paper. The first machine (Machine A) is shown in Fig. 14. It was designed without the proposed efficiency-optimization method that includes air-friction losses, but a litz-wire winding and an amorphous iron core were used. The 100-W 500 000-r/min machine is used as generator in a miniature-gas-turbine application and for driving an ultracompact turbo compressor [18], [19].

The second machine (Machine B) is shown in Fig. 15. It was designed for a rotational speed of 1 000 000 r/min and a shaft power of 100 W, using the efficiency-optimization method that includes air-friction losses. Both machines are manufactured equally and have rotors that are supported by the same high-speed ball bearings. The bearing selection and losses are not part of the analysis in this paper as the bearing losses are independent of the optimization parameters, and the bearing selection depends strongly on the application.

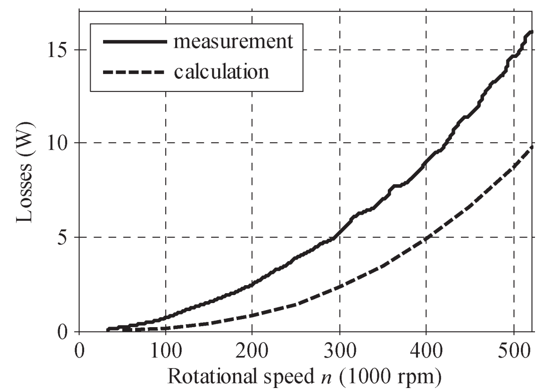

Fig. 16. Results of Machine A. L1osses measured by means of (solid) deceleration test and (dashed) calculated losses. The measured losses include the proximity-effect, iron, air-friction, and bearing-friction losses. The calculated losses include the proximity-effect, iron, and air-friction losses. The current-dependent resistive losses $P_{\mathrm{Cu},s}$ are excluded in both cases.

B. Measurements

It is not easy to measure the losses of a machine having a very low torque and a very high speed (in the millinewton-meter region and above 100 000 r/min), the loss measurement being a field of research itself [20], [21]. A rotary torque transducer is not feasible due to the high speed, and reaction torque measurement of very small torque differences offers insufficient accuracy. Therefore, the deceleration test is the preferred method [16]. For the measurements, the rotor was accelerated to a certain speed, after which the drive system was switched off, letting the losses decelerate the rotor. The speed was recorded as a function of time, and the losses were calculated afterward using the known moment of inertia of the rotor.

The measured losses include the proximity-effect, iron, air-friction, and bearing-friction losses. The current-dependent resistive losses $P_{\mathrm{Cu},s}$ are excluded, but they can be estimated very accurately by using the measured dc resistance, since the skin effect is negligible due to the litz wire. The bearing-friction losses are included in the measurement but not included in the total losses P_d that are calculated in the optimization procedure. Estimating the friction losses of ball bearings is difficult because these losses depend on the age of the bearings, the axial preload, the temperature, and the unbalance of the rotor.

The measured and calculated losses of Machine A are shown in Fig. 16, and the corresponding losses of Machine B are shown in Fig. 17. It is to be noted that the calculated losses do not include the bearing-friction losses. The manufacturer's estimate is 5 W for the two bearings at 500 000 r/min, which corresponds well to the results shown in Figs. 16 and 17. It can be seen that the losses can be drastically reduced by decreasing the rotor diameter. This reduction is mainly due to decreased air-friction losses, which are proportional to the power of four of the rotor radius in (3).

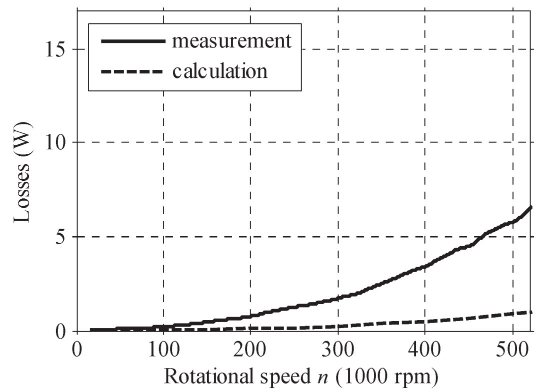

Fig. 17. Results of Machine B. Losses measured by means of (solid) deceleration test and (dashed) calculated losses. Explanations of the loss components are as in Fig. 16.

TABLE II
LOSS-REDUCTION CONTRIBUTIONS

Change of	Old	New	Loss reduction
Magnet radius R_1	2.5 mm	1.7 mm	5.2 W
Inner radius R_4 of stator core	5.5 mm	5.3 mm	0 W
Air gap $R_3 - R_2$	0.5 mm	0.2 mm	0.7 W
Sleeve thickness $R_2 - R_1$	0.5 mm	0.25 mm	1.3 W
Iron core material	SiFe	amorphous	1.8 W

VIII. CONCLUSION

Analytical models can be used for the optimization of high-speed PM machines that are equipped with a diametrically magnetized rotor and a slotless stator. In the efficiency optimization of an ultrahigh-speed machine, the air-friction losses have to be taken into account in addition to the usual iron, copper, and eddy-current losses. In this paper, general analytical models were presented for the field calculation and loss components, and a loss-minimization procedure is applied for selecting the internal dimensions of the machine.

The calculated losses of an existing 100-W 500 000-r/min machine, designed without considering air friction, are 14.2 W. The optimization of the magnet radius and the inner radius of the stator core results in a reduction of the losses by 5.2 W. The minimization of the sleeve thickness and air gap further reduces the losses by 2 W, whereas the improvement by optimizing the already thin litz-wire strand diameter is negligible. Changing the core material from silicon–iron to amorphous iron laminations decreases the losses by another 1.8 W. The loss-reduction contributions obtained by the different changes are compiled in Table II. The final machine design has 5.2-W total losses, which is 63% lower than those of the existing machine.

It can be concluded that, for a loss-minimizing design, the proximity-effect losses and the air-friction losses have to be taken into account in an ultrahigh-speed machine with a slotless stator. The proximity-effect loss calculation leads to a litz-wire winding with a small strand diameter and, including the air-friction losses, results in a small magnet radius. In addition to low losses, the use of a high-frequency stator core material—such as amorphous iron—allows for a smaller outer diameter of the stator with an insignificant increase in the total losses. Deceleration measurements of existing prototypes proved that the losses in ultrahigh-speed operation can be drastically reduced by decreasing the rotor diameter, mainly due to the lower air-friction losses.

Increasing the speed toward 1 000 000 r/min results in machines with decreasing magnet, shaft, and stator radii. For designing machines to be integrated into various applications, the efficiency optimization has to be coupled with the rotor dynamic and thermal analyses. Results of research in this direction will be published in a future paper.

APPENDIX

A. Magnetic Field Problem Formulation

A 2-D boundary-value problem is formulated for the magnetic field, and the effects of the third dimension are ignored. The polar r–θ coordinate system fixed to the rotor cross section is shown in Fig. 1. The diametrically magnetized PM has a uniformly distributed remanence flux density $\mathbf{B}_{\text{rem}}$ in the direction of $\theta = 0$. The magnetic flux density is given by

$$\boldsymbol{B} = \mu_0 \boldsymbol{M}_p + \mu_r \mu_0 \boldsymbol{H} \tag{10}$$

where $\mathbf{M}_p$ is the permanent magnetization, $\mathbf{H}$ is the magnetic field strength, and μ_r is the relative recoil permeability.

The problem region is divided into three subregions. In the PM region $(0 \le r \le R_1)$, $\mathbf{M}_p = \mathbf{B}_{\text{rem}}/\mu_0$, and $\mu_r = \mu_{r1}$. The uniform permanent magnetization is given by

$$\boldsymbol{M}_p = \mathbf{u}_r M_p \cos\theta - \mathbf{u}_\theta M_p \sin\theta \tag{11}$$

where $\mathbf{u}_r$ and $\mathbf{u}_\theta$ are the radial and azimuthal unit vectors, respectively. In the nonferromagnetic region between the PM and the stator core $(R_1 < r < R_4)$, $\mathbf{M}_p = 0$, and $\mu_r = 1$. In the stator core $(R_4 < r < R_5)$, $\mathbf{M}_p = 0$, and $\mu_r = \mu_{r5}$.

The magnetic field is modeled by means of the magnetic scalar potential ϕ defined by $\mathbf{H} = -\nabla\phi$. Inserting this definition with (10) into the governing equation $\nabla \cdot \mathbf{B} = 0$ yields the Laplace equation $\nabla^2\phi = 0$ for the scalar potential. It is to be noted that $\nabla \cdot \mathbf{M}_p = 0$ for uniform permanent magnetization.

In the polar-coordinate system, the partial differential equation of the scalar potential is

$$\frac{\partial^2\phi}{\partial r^2} + \frac{1}{r}\frac{\partial\phi}{\partial r} + \frac{1}{r^2}\frac{\partial^2\phi}{\partial\theta^2} = 0. \tag{12}$$

In addition to the partial differential equation, interface and boundary conditions have to be defined. The continuity of the tangential component of the magnetic field strength requires that ϕ is continuous over the interfaces at R_1 and R_4. The continuity of the normal component of the magnetic flux density requires that $M_p \cos\theta - \mu_r \partial\phi/\partial r$ is continuous over the interfaces at R_1 and R_4. The normal component of the magnetic flux density vanishes at the outer boundary of the machine, which gives the boundary condition $-\mu_r \partial\phi/\partial r = 0$ at R_5.

B. Magnetic Field Solution

Expressions for the magnetic field are obtained in the whole machine by solving the problem consisting of the partial differential equation (12) and the interface and boundary conditions. The solution can be obtained by separation of variables. In the PM $(0 \le r \le R_1)$, the radial and azimuthal components of the magnetic flux density are

$$B_r = K_{B1}\cos\theta \quad B_\theta = -K_{B1}\sin\theta \tag{13}$$

respectively, where the flux density coefficient is

$$K_{B1} = \frac{B_{\mathrm{rem}}}{N}\left[\left(1-\frac{R_4^2}{R_5^2}\right)\left(1+\frac{R_1^2}{R_4^2}\right) + \frac{1}{\mu_{\mathrm{r}5}}\left(1+\frac{R_4^2}{R_5^2}\right)\left(1-\frac{R_1^2}{R_4^2}\right)\right] \tag{14}$$

with the definition

$$N=\left[1-\left(\frac{R_4}{R_5}\right)^2\right]\left[(\mu_{r1}+1)-(\mu_{r1}-1)\left(\frac{R_1}{R_4}\right)^2\right] + \frac{1}{\mu_{r5}}\left[1+\left(\frac{R_4}{R_5}\right)^2\right]\left[(\mu_{r1}+1)+(\mu_{r1}-1)\left(\frac{R_1}{R_4}\right)^2\right]. \tag{15}$$

In the nonferromagnetic region $(R_1 \le r \le R_4)$, the radial and azimuthal components of the magnetic flux density are

$$B_r = K_{B2}\left[1+\left(\frac{R_4}{r}\right)^2\right]\cos\theta$$
$$B_\theta = -K_{B2}\left[1-\left(\frac{R_4}{r}\right)^2\right]\sin\theta \tag{16}$$

respectively, where the flux density coefficient is

$$K_{B2}=\frac{B_{\mathrm{rem}}}{N}\left\{\left[1-\left(\frac{R_4}{R_5}\right)^2\right]-\frac{1}{\mu_{r5}}\left[1+\left(\frac{R_4}{R_5}\right)^2\right]\right\}\left(\frac{R_1}{R_2}\right)^2. \tag{17}$$

In the stator core $(R_4 \le r \le R_5)$, the components of the magnetic flux density are

$$B_r = K_{B3}\left[-1+\left(\frac{R_5}{r}\right)^2\right]\cos\theta$$
$$B_\theta = -K_{B3}\left[1+\left(\frac{R_5}{r}\right)^2\right]\sin\theta \tag{18}$$

respectively, where the flux density coefficient is

$$K_{B3} = \frac{2B_{\mathrm{rem}}}{N}\left(\frac{R_1}{R_5}\right)^2. \tag{19}$$

C. Torque Calculation

The density of the azimuthal-force component caused by the spatial fundamental wave J_1 of the current density in the stator winding is $J_1 B_r$. The electromagnetic torque is obtained as the integral

$$T_e = L\int_{-\pi}^{\pi}\int_{R_3}^{R_4} r^2 J_1 B_r\, dr\, d\theta. \tag{20}$$

The stator-current component in the direction of the PM flux is controlled to zero. Using (16), the integration in (20) results in

$$T_e = \sqrt{2}\pi k_w k_{\mathrm{Cu}} J K_{B2} L R_4^3\left(\frac{4}{3}-\frac{R_3}{R_4}-\frac{1}{3}\frac{R_3^3}{R_4^3}\right) \tag{21}$$

where k_w is the fundamental-wave winding factor, k_{Cu} is the winding fill factor, and J is the rms current density in the conductors.

The current density J can be solved from (21) if the electromagnetic torque is known for an operating point. The winding factor for the distributed three-phase air-gap winding shown in Fig. 1 is

$$k_w = \frac{6}{\pi}\sin\frac{\pi}{6}. \tag{22}$$

REFERENCES

[1] M. A. Rahman, A. Chiba, and T. Fukao, "Super high speed electrical machines—Summary," in *Proc. IEEE Power Eng. Soc. Gen. Meeting*, Jun. 6–10, 2004, vol. 2, pp. 1272–1275.

[2] C. Zwyssig, S. D. Round, and J. W. Kolar, "Analytical and experimental investigation of a low torque, ultra-high speed drive system," in *Conf. Rec. 41st IEEE IAS Annu. Meeting*, Tampa, FL, Oct. 8–12, 2006, vol. 3, pp. 1507–1513.

[3] C. Zwyssig, J. W. Kolar, W. Thaler, and M. Vohrer, "Design of a 100 W, 500 000 rpm permanent-magnet generator for mesoscale gas turbines," in *Conf. Rec. 40th IEEE IAS Annu. Meeting*, Hong Kong, Oct. 2–6, 2005, vol. 1, pp. 253–260.

[4] J. D. Ede, Z. Q. Zhu, and D. Howe, "Optimal split ratio for high-speed permanent magnet brushless DC motors," in *Proc. Int. Conf. Elect. Mach. Syst.*, Shenyang, China, 2001, pp. 909–912.

[5] N. Bianchi, S. Bolognani, and F. Luise, "Potentials and limits of high-speed PM motors," *IEEE Trans. Ind. Appl.*, vol. 40, no. 6, pp. 1570–1578, Nov./Dec. 2004.

[6] Z. Q. Zhu, D. Howe, E. Bolte, and B. Ackermann, "Instantaneous magnetic field distribution in brushless permanent magnet dc motors, Part I: Open-circuit field," *IEEE Trans. Magn.*, vol. 29, no. 1, pp. 124–135, Jan. 1993.

[7] U. Kim and D. K. Lieu, "Magnetic field calculation in permanent magnet motors with rotor eccentricity: Without slotting effect," *IEEE Trans. Magn.*, vol. 34, no. 4, pp. 2243–2252, Jul. 1998.

[8] K. F. Rasmussen, J. H. Davies, T. J. E. Miller, M. I. McGilp, and M. Olaru, "Analytical and numerical computation of air-gap magnetic fields in brushless motors with surface permanent magnets," *IEEE Trans. Ind. Appl.*, vol. 36, no. 6, pp. 1547–1554, Nov./Dec. 2000.

[9] Z. Q. Zhu, D. Howe, and C. C. Chan, "Improved analytical model for predicting the magnetic field distribution in brushless permanent-magnet machines," *IEEE Trans. Magn.*, vol. 38, no. 1, pp. 229–238, Jan. 2002.

[10] T. Modeer, "On stator yoke rotational iron losses in permanent magnet machines," presented at the Int. Conf. Electrical Machines (ICEM), Chania, Greece, Sep. 2–5, 2006, 5 pp, Paper OTA4-1.

[11] L. Atallah, Z. Q. Zhu, D. Howe, and T. Birch, "Armature reaction field and winding inductances of slotless permanent-magnet brushlesss machines," *IEEE Trans. Magn.*, vol. 34, no. 5, pp. 3737–3744, Sep. 1998.

[12] K. Ng, Z. Q. Zhu, and D. Howe, "Open-circuit field distribution in a brushless motor with diametrically magnetized PM rotor, accounting for slotting and eddy current effects," *IEEE Trans. Magn.*, vol. 32, no. 5, pp. 5070–5072, Sep. 1996.

[13] R. Holm, H. Polinder, and J. A. Ferreira, "Analytical modeling of a permanent-magnet synchronous machine in a flywheel," *IEEE Trans. Magn.*, vol. 43, no. 5, pp. 1955–1967, May 2007.

[14] J. A. Ferreira, *Electromagnetic Modeling of Power Electronic Converters*. Norwell, MA: Kluwer, 1989.

[15] X. Nan and C. R. Sullivan, "An equivalent complex permeability model for Litz-wire windings," in *Conf. Rec. 40th IEEE IAS Annu. Meeting*, Hong Kong, Oct. 2–6, 2005, vol. 3, pp. 2229–2235.

[16] M. Mack, "Luftreibungsverluste bei Elektrischen Maschinen kleiner Baugrösse," Ph.D. dissertation, Universität Stuttgart, Stuttgart, Germany, 1967.

[17] "Pack Feindrähte," Litz Wire Table, May 2, 2007. [Online]. Available: http://www.pack-feindraehte.de

[18] B. Schneider, M. Bruderer, D. Dyntar, C. Zwyssig, M. Diener, K. Boulouchos, R. S. Abhari, L. Guzzella, and J. W. Kolar, "Ultra-high-energy-density converter for portable power," in *Proc. Int. Workshop Micro Nanotechnol. Power Generation Energy Convers. Appl.*, Tokyo, Japan, Nov. 28–30, 2005, pp. 81–84.

[19] C. Zwyssig, D. Krähenbühl, H. Weser, and J. W. Kolar, "A miniature turbocompressor system," in *Proc. Smart Energy Strategies*, Zurich, Switzerland, Sep. 2008, pp. 144–149.

[20] V. Gass, B. H. van der Schoot, S. Jeanneret, and N. F. de Rooij, "Micro-torque sensor based on differential force measurement," in *Proc. IEEE Workshop Micro Electro Mech. Syst.*, Oiso, Japan, Jan. 25–28, 1994, pp. 241–244.

[21] H. Ota, T. Ohara, Y. Karata, S. Nakasima, and M. Takeda, "Novel micro torque measurement method for microdevices," *J. Micromech. Microeng.*, vol. 11, no. 5, pp. 595–602, Sep. 2001.

Jorma Luomi (M'92) received the M.Sc. (Eng.) and D.Sc. (Tech.) degrees from Helsinki University of Technology, Espoo, Finland, in 1977 and 1984, respectively.

In 1980, he joined Helsinki University of Technology. From 1991 to 1998, he was a Professor at Chalmers University of Technology, Göteborg, Sweden. He is currently a Professor in the Department of Electrical Engineering, Helsinki University of Technology. His research interests are in the areas of electric drives, electric machines, and numerical analysis of electromagnetic fields.

Christof Zwyssig (S'05) studied electrical engineering at the Swiss Federal Institute of Technology (ETH) Zürich, Zürich, Switzerland, where he received the M.Sc. and Ph.D. degrees in 2004 and 2008, respectively. He studied power electronics, machines, and magnetic bearings and was engaged in research on high-speed electrical drive systems and their power electronics.

He was also with Chalmers University of Technology, Sweden, where he was involved in the field of wind turbines. Since January 2009, he has been with Celeroton, Zürich, Switzerland, a spin-off company in the area of high-speed electrical drive systems, where he is a co-founder.

Andreas Looser (S'08) received the M.Sc. degree in electrical engineering, focusing on electrical-drive systems, power electronics, and very large scale integration, from the Eidgenoessische Technische Hochschule (ETH) Zürich, Zürich, Switzerland, in 2007, where he has been working toward the Ph.D. degree with a focus on high-speed electrical drives and bearing technology in the Power Electronic Systems Laboratory since 2008.

He has also been working as a Research Associate in the Power Electronic Systems Laboratory.

Johann W. Kolar (SM'04) received the Ph.D. degree (*summa cum laude*) in industrial electronics from the University of Technology Vienna, Vienna, Austria.

From 1984 to 2001, he was with the University of Technology Vienna, where he taught and worked on research in close collaboration with industry. He has proposed numerous novel converter topologies, e.g., the VIENNA Rectifier and the Three-Phase AC–AC Sparse Matrix Converter concept. He has published over 200 scientific papers in international journals and conference proceedings and has filed more than 50 patents. He was appointed Professor and Head of the Power Electronics Systems Laboratory, Eidgenoessische Technische Hochschule Zürich, Zürich, Switzerland, on February 1, 2001. The focus of his current research is on ultracompact intelligent ac–ac and dc–dc converter modules employing the latest power semiconductor technology (SiC), novel concepts for cooling and active electromagnetic-interference filtering, multidisciplinary simulation, bearingless motors, power microelectromechanical systems, and wireless power transmission.